CHAPTER 9

Metallic and Plasmonic Nanolasers

Martin T. Hill

Contents

1. INTRODUCTION

Reducing the size of lasers and other photonic devices produces benefits similar to those seen with the shrinking dimensions of electronic components. A smaller laser requires less power and can potentially be switched on and off faster. The vertical-cavity surface-emitting laser (VCSEL) (Iga, 2000) is an example of this miniaturization process. This was the first laser with a wavelength scale optical mode, and it is being employed in an increasing number of applications. Most recent research in nanolasers has been into photonic crystal cavity lasers (Painter *et al.*, 1999) Here the light is confined strongly in two dimensions by what are effectively

P.O. Box 2258, Warwick, WA, Australia

Semiconductors and Semimetals, Volume 86
ISSN 0080-8784, DOI: 10.1016/B978-0-12-391066-0.00009-5

two-dimensional Bragg mirrors formed by making a pattern of holes in a high-refractive index semiconductor. All of these cavities exploit refractive index differences of dielectric materials to confine the light. The smallest dimensions to which the optical mode of such cavities can be confined are related to the diffraction limit and are on the order of one-half of the wavelength of light in the dielectric material. Further, in order to be effective, the dielectric mirror structure typically has to be many wavelengths in size, implying that the total laser size is still large compared to the wavelength of light.

In theory, it is possible to use metals to form the laser resonator. The metal may form either strong compact mirrors, able to confine light to about the size of the diffraction limit. Alternatively, the light may interact strongly with the free electrons in the metal, being guided in the form of surface plasmon polaritons (SPPs) at the interface between a metal (conductor) and a dielectric (nonconducting) material such as air (Atwater, 2007; Barnes *et al.*, 2003). Structures employing this form of light confinement have minimum size scales related to the penetration depth of light into the metal, which is typically of the order of tens of nanometers. Unfortunately, the metal conduction electrons which oscillate in synchronism with the optical field dissipate energy through collisions with the metal's atomic lattice. This energy dissipation leads to high-optical losses, so SPPs can only travel short distances and metal mirrors have higher losses than dielectric ones. However, a number of workers did examine the possibility of using gain in metallic waveguides (Maier, 2006; Maslov and Ning, 2007; Nezhad *et al.*, 2004).

In the last couple of years, efforts to use metals to form the nanolaser resonator have shown that it is possible for optical gain medium to compensate the high-optical losses. Further, metals have allowed both the overall size of the laser to be reduced to smaller than the wavelength of light and the optical mode dimensions to be reduced below the diffraction limit. Some of these devices are coming close to being useful light sources, and it may only be a few years before we see lasers based on metallic nanostructures in applications. Metallic or plasmonic nanolasers could become technologically significant, particularly when the laser and mode size can be reduced far below the diffraction limit. Some of the major reasons for this significance are as follows: (1) There is a perceived need for small, fast low-power lasers to cope with the increasing bandwidth of inter- and intra-integrated circuit communications (Miller, 2009). (2) New applications may appear based on the ability to make arrays of coherent emitters with subwavelength pitch. (3) These metallic devices could offer improved light emitters compared to dielectric cavity devices, particularly for the longer wavelengths. (4) Ultra high-speed low-power lasers may open up the possibility for optical signal processing that is competitive with electronics in the high performance region. (5) Finally,

these devices will also be important sources and amplifiers for subwavelength plasmonic circuits.

This chapter has been written with the following goals in mind: (1) to provide an introduction to the critical issues and methods involved in designing metallic nanolasers; (2) to give a review of the progress and provide a list of the important references; and (3) to provide an overview of the various designs which will hopefully give some motivation to further development and innovation.

To this end, the chapter is organized as follows: In Section 2, a model for metals and some significant modes which occur in plasmonic laser devices are discussed. Section 3 looks at a simple model of optical gain in these devices and works through some examples on the amount of gain required for various metallic laser devices. Section 4 looks at most of the various designs used to achieve lasing in metallic nanostructures. Emphasis is given to metal-clad structures, and also some of the technology details involved with these devices are discussed. Finally, a look at future directions and conclusions are given in Section 5.

2. METALS AND SURFACE MODES

The common characteristic of all the devices described in this chapter is that the cavities are formed from metals. Most metals at optical frequencies can be described by a complex relative permittivity: $\varepsilon_m = \varepsilon'_m + j\varepsilon''_m$. In general, ε_m is a complex function of wavelength. However, for metals of interest, and for light wavelengths including the near infrared and most of the visible range, the response of the metal to the applied electromagnetic field is determined primarily by the motion of free electrons in the metal. The optical response can be described by the Drude or free electron model (Omar, 1975), as a function of the radian frequency of interest ω:

$$\varepsilon_m(\omega) = 1 - \frac{\omega_p^2}{\omega(\omega + j\gamma)} \tag{9.1}$$

Furthermore, ω_p is the so-called plasma frequency of the metal, and γ the damping rate (Omar, 1975). From Eq. (9.1), it can be seen that for frequencies below the plasma frequency ε_m is negative. This leads to an intrinsic wave impedance $\sqrt{\mu/\varepsilon}$ being predominately imaginary (Ramo *et al.*, 1984), and light waves impeding on the metal from a dielectric are reflected.

Apart from forming strong mirrors, light waves can become trapped at the metal–dielectric interface and propagate along this surface. The light waves are trapped by their interaction with the free electrons, which respond collectively by oscillating in resonance with the light wave (Fig. 9.1A). These light waves and free electron oscillations which

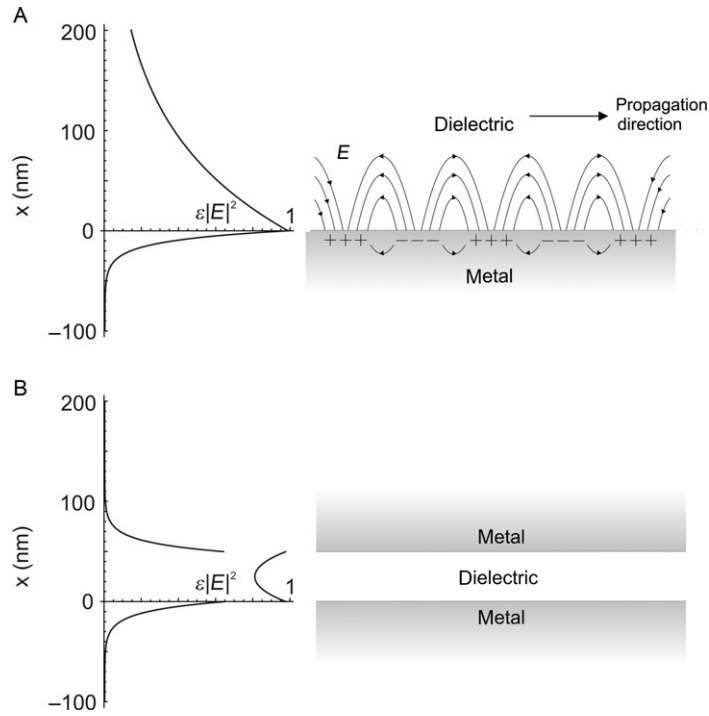

FIGURE 9.1 (A) Schematic view of the interaction of the electric field (red lines) and the surface charges caused by the movement of free electrons for surface plasmon polariton (SPP) that moves along the interface between a metal and dielectric. Also shown is a plot of the energy in the electric field at a distance *x* (in nm) from the metal–dielectric interface, this was calculated for InGaAs as the dielectric and silver metal, at a wavelength of 1.55 μm. Note that for wavelengths far from the metal plasma resonance the SPP is not so strongly confined at the metal surface. (B) Schematic of a metal–insulator–metal (MIM) waveguide. The insulator thickness is 50 nm. Also shown is a plot of the energy in the electric field at a distance *x* (in nm) from the first metal–dielectric interface, for the same materials and wavelength as in (A). Note the much stronger confinement of the electromagnetic energy. Electric field energy in the metal is defined as in Loudon (1970).

propagate along the surface of the metal are called surface plasmons (SPPs) (Barnes *et al.*, 2003). Uniquely these waves permit resonant cavities to be formed where the light is concentrated into subwavelength volumes, and the resonant cavities can have sizes smaller than the diffraction limit in one or more dimensions.

For the purpose of illustration, field profiles of a few important SP modes with analytical solutions are given here. First consider a single metal insulator interface as shown in Fig. 9.1A. The magnitude of the electric field $|E|^2$ of the surface plasmon mode traveling along the

interface as a function of the distance from the interface x can be found to be (Chuang, 2009):

$$|E|^2 = \begin{cases} |\mu_0/(\varepsilon_0\varepsilon_g)|e^{-\alpha_g x}, & x > 0 \\ |\mu_0/(\varepsilon_0\varepsilon_m)|e^{-\alpha_m x}, & x \leq 0 \end{cases} \tag{9.2}$$

$$\alpha_g = \frac{4\pi}{\lambda}\sqrt{-\frac{\varepsilon_g^2}{\varepsilon_g + \varepsilon_m}} \tag{9.3}$$

$$\alpha_m = \frac{4\pi}{\lambda}\sqrt{-\frac{\varepsilon_m^2}{\varepsilon_g + \varepsilon_m}} \tag{9.4}$$

In Fig. 9.1A, a representative field profile is given for the case of silver metal with InGaAs as the dielectric with a relative permittivity ε_g=12.96, at a wavelength λ of 1.55 μm. Here the electromagnetic energy density ($\varepsilon_0\varepsilon_g|E|^2$ for the dielectric) is plotted as a function of distance from the metal/dielectric interface. It can be seen that although the electric field extends a distance of approximately a quarter wavelength into the dielectric, into the metal the field drops off much more rapidly.

A second metal/insulator interface can be introduced by creating either insulator–metal–insulator or metal–insulator–metal (MIM) planar structures (Dionne *et al.*, 2006; Prade *et al.*, 1991). The focus here is on the MIM structure. The even lowest-order transverse magnetic (TM_0) mode propagated by the MIM waveguide is shown in Fig. 9.1B. Here the energy density is plotted as a function of distance x from the bottom metal/dielectric interface for a specific example of silver with InGaAs insulator core, and a core width of 50 nm. The general analytical solutions for MIM waveguides can be found in (Prade *et al.*, 1991). The TM_0 mode is important because, even as the insulator thickness is made arbitrarily small, the mode can still propagate. Note that the electric field is tightly confined inside the core and that the field in the metal drops off at a greater rate than in the single-interface SP mode.

In general, the metal and dielectric nanolaser cavity will have a more complex structure than the above examples. Additionally, slight deviations from the desired form can lead to significant changes in the cavity mode. So numerical methods such as finite element mode solvers or finite difference time-domain techniques (Taflove and Hagness, 2005) offer the best approach to obtain the cavity-mode profile.

For the purpose of simulation, the relative permittivity, and hence the Drude model parameters ω_p and γ, describing the metal of interest, can be obtained from tables of optical measurements (Johnson and Christy, 1972; Palik 1997; Theye, 1970). It should be noted that there can be a considerable difference between published values of ε_m, in particular due to significant differences in the damping rate γ found by different authors.

These differences can occur due to the sample preparation methods and the measurement technique employed. It has been shown that for gold the damping rate γ can depend strongly on the crystal structure (Kuttge *et al.*, 2008). The disorder in the metal crystal lattice at grain boundaries increases the scattering losses seen by electrons (Kuttge *et al.*, 2008). In fact, recent devices made from single crystal gold have shown greatly improved performance than those made with evaporated gold (Huang *et al.*, 2010a). The metal crystal structure can be greatly affected by the deposition technique, deposition thickness, and annealing of the metal after deposition. Another aspect to be considered is the surface roughness of the metal. In the literature, the roughness of the surface on which the SPs are traveling has been identified as important. Deposition of seed layers of germanium or nickel has been shown to improve the surface roughness (Liu *et al.*, 2010). In other structures, such as the encapsulated metal structures that will be looked at later, the metal surface which interacts with the light is the surface at which metal deposition is started. Effectively, the metal is deposited onto a form and it is the inside surface where the optical mode resides. It has been shown that very smooth metal surfaces can be obtained at this internal metal/dielectric interface (Nagpal *et al.*, 2009).

A final aspect of the metal is the change in optical loss with temperature. The imaginary component of the permittivity ε''_m is responsible for the metal absorption losses (Omar, 1975). According to the free electron model of metals (Omar, 1975; Theye, 1970), ε''_m decreases with temperature due to reduced free electron–phonon scattering in the metal. More specifically, the electron relaxation time in the metal, on which ε''_m depends, increases with decreased temperature (Omar, 1975). The direct current electrical conductivity of the metal is also proportional to the electron relaxation time (Omar, 1975; Theye, 1970). Although the optical properties of noble metals such as gold follow roughly the free electron model, there are discrepancies (Theye, 1970). Discrepancies have been found between the electron relaxation times deduced from optical and electrical measurements (Theye, 1970). However, there have been a number of experiments with nanolasers that seem to indicate that the optical losses of metals are substantially reduced at cryogenic temperature (Hill *et al.*, 2007; Kwon *et al.*, 2010; Lakhani *et al.*, 2011; Yu *et al.*, 2010). Other experiments do not show a strong temperature dependence on the losses (Mayy *et al.*, 2009); however, the metal crystal structure may have a significant bearing on the temperature dependence of losses. In (Hill *et al.*, 2007; Lakhani *et al.*, 2011) an estimate of the low temperature, ε''_m was obtained by assuming the free electron model is valid, and the room temperature (RT) ε''_m is scaled by a factor of the RT conductivity divided by the low-temperature conductivity.

3. OPTICAL GAIN

The second component in any laser, after the resonant cavity, is the optical gain medium required to overcome optical losses. Examples of gain medium are certain dyes (Knobbe *et al.*, 1980; Yarborough, 1974), semiconductors (Chuang, 2009), and doped crystals (Albrecht *et al.*, 1985; Noginov *et al.*, 2000). Again, the relative permittivity of the gain medium at a particular frequency can be described by a complex number: $\varepsilon_g = \varepsilon'_g + j\varepsilon''_g$, where ε''_g is negative. Depending on the particular material, various models are used to give ε_g as a function of wavelength (Chuang, 2009). A rather simple but useful approximation for the gain medium relative permittivity is to employ a classical Lorentz model (Taflove and Hagnes, 2005):

$$\varepsilon_g(\omega) = \varepsilon_{\infty g} + \frac{\Delta\varepsilon_g \omega_g^2}{\omega_g^2 - j\Gamma_g \omega - \omega^2} \tag{9.5}$$

where ω_g is the frequency of maximum gain, $\varepsilon_{\infty g}$ is the relative permittivity far from the gain maximum, and Γ_g is the damping factor, $\Delta\varepsilon_g$ is the interaction strength between the oscillators and the electromagnetic field, which in the case of optical gain is negative. Figure 9.2 shows a plot of the real and imaginary permittivities.

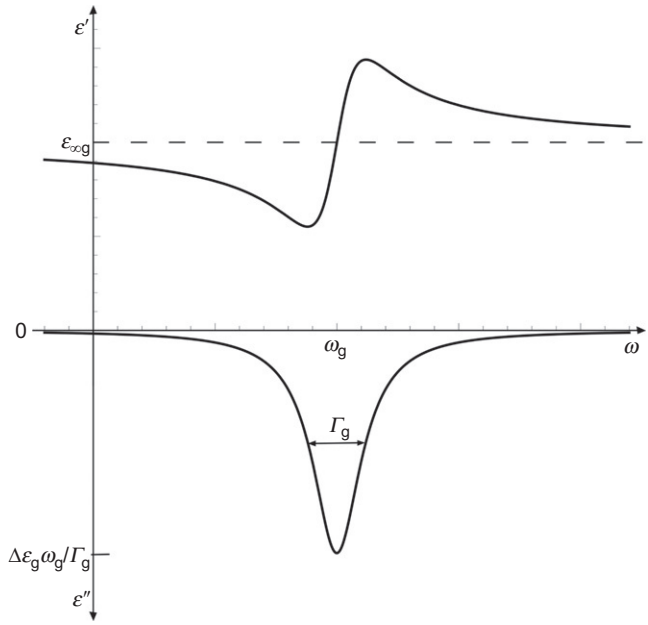

FIGURE 9.2 Plot of the relative permittivity, both the real ε' and imaginary ε'' parts for a gain medium described by a Lorentz model.

The key issue in metallic nanolasers is how much gain is required to overcome the significant metal-induced losses in the cavity. To determine the required material gain, the quality factor Q of the cavity, and how much of the optical mode overlaps the gain medium need to be known. For waveguide structures, there have been several papers looking at this aspect of energy confinement and the propagation of energy (Chang and Chuang, 2009; Chang *et al.*, 2010a,b,c). Due to dispersion and the negative refractive index of the metal, the calculation of the optical mode overlap in the gain medium and the threshold gain can be more complicated than for dielectrics (Visser *et al.*, 1997). Further, in many of the devices discussed later, the gain required is so high that often the gain medium dispersion becomes significant and dominates the energy storage in the cavity.

Here, a simple approach is taken that can be used on arbitrarily shaped cavities, takes into account dispersion of the gain medium, and evaluates energy storage consistently in the metal and gain medium. The permittivity of the metal can be described also by a Lorentz model as the Drude model is just a limiting case of a Lorentz model (Judkins and Ziolkowski, 1995). With the model constants for metal being ω_m, $\varepsilon_{\infty g}$, $\Delta\varepsilon_m$, Γ_m. The relation of the Lorentz to the Drude parameters is (Judkins and Ziolkowski, 1995): $\Delta\varepsilon_m \gg 1$, $\Gamma_m = \gamma$, $\omega_m = \omega_p/\sqrt{\Delta\varepsilon_m}$, $\varepsilon_{\infty m} = 1$.

The index of refraction n and the extinction coefficient κ are related to the permittivity by:

$$n_i + j\kappa_i = \sqrt{\varepsilon_i(\omega)}, \quad i \in m, g \tag{9.6}$$

The electromagnetic energy density $\overline{W_i}$ stored in a material, which has a permittivity described as in Eq. (9.5) can be shown to be (Loudon, 1970):

$$\overline{W_i} = \frac{\varepsilon_0}{2}\left(n_i^2 + \frac{2\omega n_i \kappa_i}{\Gamma_i}\right)|E_i|^2, \quad i \in m, g \tag{9.7}$$

where $|E|$ is the magnitude of the electric field at the point the energy density is being measured. Furthermore, the relaxation time T_i which determines the time rate of decay of energy in the medium at a particular frequency ω is given in Loudon (1970) as:

$$\frac{1}{T_i} = \frac{4\omega^2\Gamma_i A_i^2}{\left[\left\{\left(\omega_i^2 - \omega^2\right)^2 + \omega^2\Gamma_i^2\right\}^{1/2} + \left\{\left(\omega_i^2 - \omega^2 + A_i^2\right)^2 + \omega^2\Gamma_i^2\right\}^{1/2}\right]^2 + 4\omega^2 A_i^2 - A_i^4} \tag{9.8}$$

$$A_i^2 = \frac{\Delta\varepsilon_i \omega_i^2}{\varepsilon_{\infty i}}, \quad i \in m, g \tag{9.9}$$

Typically, a laser cavity will consist of some metal, the gain medium and also some inactive dielectric which is modeled by a simple refractive

index $\sqrt{\varepsilon_d}$. Mode solvers or time-domain simulations can determine the mode profile for the lasing mode, given a cavity or waveguide design. Also the decay time of the mode can be found T_c. The losses come from either the metal or radiation losses. From the mode profile, $|E|$ can be found over the whole cavity, and by integrating the energy densities $\overline{W_i}$ over their component materials, the electromagnetic energy stored in each material W_i can be found. The relaxation time for the metal T_m is known at the cavity resonant frequency ω from the model parameters derived from refractive index and extinction coefficient data (Johnson and Christy, 1972). If there are only metallic losses in the system, then $T_c{=}T_m(W_m{+}W_d{+}W_g)/W_m$, where $W_m{+}W_d{+}W_g$ is the total energy in the modal field. Assuming that the dielectric material is lossless, if the optical gain exactly compensates the losses, the following must be true:

$$T_g\left(\Delta\varepsilon_g, \Gamma_g, \omega\right) = \frac{-T_c W_g\left(\Delta\varepsilon_g, \Gamma_g, \omega\right)}{W_m + W_d + W_g\left(\Delta\varepsilon_g, \Gamma_g, \omega\right)} \tag{9.10}$$

Assuming that the device operates at the semiconductor gain peak, that is, $\omega{=}\omega_g$, and that the *only* source of loss is the metal, then Eq. (9.10) simplifies to the following which relates the interaction strength between the oscillators and the electromagnetic field $\Delta\varepsilon_g$, to the damping Γ_g in the gain medium:

$$\Delta\varepsilon_g = \frac{W_m}{T_m}\frac{\Gamma_g}{\omega_g^2}\frac{2}{\varepsilon_0}\frac{1}{\int\int\int |E_g|^2} \tag{9.11}$$

where $\int\int\int |E_g|^2$ represents the integrated electric field intensity over the gain medium. The material gain per unit length required to overcome the metal losses is related to the gain medium complex part of relative permittivity and is given by

$$\alpha_g = \frac{2\pi}{\lambda_o}\frac{\varepsilon''_g}{\sqrt{\varepsilon'_g}} = \frac{\omega_g^2\Delta\varepsilon_g}{c\sqrt{\varepsilon_{\infty g}}\Gamma_g} = \frac{1}{c\sqrt{\varepsilon_{\infty g}}}\frac{W_m}{T_m}\frac{2}{\varepsilon_0}\frac{1}{\int\int\int |E_g|^2} \tag{9.12}$$

Thus the material gain required is independent of the gain medium bandwidth and dispersion, which is given by Γ_g. It is desirable to have α_g as small as possible, to place the minimum requirements on the gain medium. In practice, the metal properties are fixed, so the only way to reduce α_g is to choose the resonant cavity or waveguide structure's dimensions and form, and the inactive dielectric index, such that the ratio of integrated $|E_g|^2$ to integrated $|E_m|^2$ is maximized.

To give an idea of the gain required to compensate metallic loses and achieve lasing, a few examples are given. For a wavelength of 1.55 μm, the relative permittivity of silver is $-130.2{+}i3.3$ (Johnson and Christy, 1972) and is modeled with parameters: $\Gamma_m{=}3.03{\times}10^{13}$, $\Delta\varepsilon_m{=}10^4$, $\omega_m{=}1.38{\times}$

10^{14}, $\varepsilon_{\infty m}$=1. This gives T_m=33fs($\sim 1/\Gamma_m$). Considering first the case of a single silver/dielectric interface which propagates a plasmon mode (Fig. 9.1). First for $\sqrt{\varepsilon_{\infty g}} = 1.5$, the ratio of electric field in the dielectric to metal is 3347, giving a gain to compensate loss of 27 cm^{-1}. If a higher index gain medium is chosen, such as a semiconductor $\sqrt{\varepsilon_{\infty g}} = 3.6$, the electric field ratio is greatly reduced to 101 (Nezhad *et al.*, 2004) and the gain required increases to 369 cm^{-1}. In Nezhad *et al.* (2004), it is shown that for the single-interface structure, the gain required is proportional to $\varepsilon_{\infty g}^{3/2}$. For an MIM structure (Fig. 9.1B), with a width of 50nm the gain required for $\sqrt{\varepsilon_{\infty g}} = 1.5$ is 376 cm^{-1}, and for $\sqrt{\varepsilon_{\infty g}} = 3.6$, the electric field ratio is 34 and the gain required is 1097 cm^{-1}. Note that for the MIM structure, even when the insulator width is reduced for example a factor of 10 down to 5nm, the electric field ratio only worsens by a factor of 2.5. So there is the possibility of creating remarkably small lasers in such structures. Note that these gain values are for a best case scenario. Often the silver loss is several times higher (Palik, 1997), and in real configurations, the gain material only occupies a fraction of the area that is not metal.

The use of a lower refractive index gain medium dramatically reduces the gain required to overcome losses in these SP mode structures (Nezhad *et al.*, 2004). Semiconductor gain material, which has a major advantage of permitting direct electrical pumping, often has a large refractive index, on the order of 3–4. In many cases, in particular where electrical pumping is involved, there is often a thin low refractive index dielectric layer placed between the semiconductor and the metal (Hill *et al.*, 2007, 2009; Lakhani *et al.*, 2011). Due to the discontinuity in the refractive index, a large peak in the modal profile occurs in the thin dielectric region, when TM or plasmonic modes are involved. Indeed, when considering just a passive waveguide or cavity, metallic losses are reduced by the presence of the dielectric layer (Oulton *et al.*, 2008). However, the ratio of modal energy in the semiconductor to that in the metal is reduced, which in general results in a higher optical gain needed to overcome metallic losses (Chen *et al.*, 2010; Hill, 2009). So for making a laser, the placement of a thin, often necessary, low-index insulating layer between the metal and semiconductor does not help overcome metallic losses, and in the case of MIM waveguides is detrimental to the device operation.

In the following sections, we will discuss specific metallic nanolaser designs. However, some useful comments can be made on the amount of gain required to overcome metallic losses in typical structures. For structures which exploit TE-like modes and have a modal minimums at the metal surfaces, effectively exploiting the metal as a strong mirror, optical gains on the order of 100 cm^{-1} or less are required for lasing (Mizrahi *et al.*, 2008; Nezhad *et al.*, 2010). Also for long-range SPPs (Barnes *et al.*, 2003), which are weakly confined similar gains are required to overcome metallic losses. For more tightly confined modes in MIM waveguide structures

where the waveguide width can be below the diffraction limit, gains on the order of 1000–5000 cm^{-1} are required (Maier, 2006). For even stronger confinement at close to the Plasmon resonance of the metals, as occurs in, for example, the SPASER, which will be discussed later (Bergman and Stockman, 2003), gains on the order $10^5 cm^{-1}$ are required (Avrutsky, 2004; Li and Yu, 2010; Noginov *et al.*, 2009). Though these gains are high, it has been shown that both semiconductors and dyes can deliver optical gains at least up to several thousand cm^{-1}.

4. LASING STRUCTURES

This section looks at the various structures that have been used to create small lasers with metallic cavities. Attention will be given to metal-encapsulated semiconductor structures as these are perhaps the most common devices demonstrated thus far. Furthermore, they are suitable for electrical pumping, which is important for their long-term application; finally, and this area is the author's specialty. Additionaly, section 4.2 on metal-encapsulated devices also incorporates some generally applicable discussion on technology and other issues such as the Purcell effect.

4.1. Stimulated emission and low-confinement structures

This chapter is primarily concerned with small metallic laser devices, where typically one or more dimensions are smaller than the lasing wavelength, and in the order of a few hundred nanometers or less. However, the initial experiments and modeling of introducing gain to metal structures were for large structures with surface plasmon modes. For completeness, a brief description of the progress and references to the major achievements are given here. The incorporation of a generic gain medium with a single-interface SPP was first theoretically studied in 1979 (Plotz *et al.*, 1979). Other more recent studies have also looked at employing specifically semiconductor gain medium (Nezhad *et al.*, 2004) and predict a material gain of $\sim 1200 cm^{-1}$ for a semiconductor gain medium is required to compensate metal losses. Lasing with SPPs was actually initially demonstrated in the late 1990s at far infrared wavelengths (Sirtori *et al.*, 1998), using quantum cascade semiconductor gain medium. At these long wavelengths $\sim 12 \mu m$, metal losses are considerably reduced. However, such devices cannot be considered micro or nanolasers.

In 2005, experiments involving thick silver films with dye gain medium showed stimulated emission of SPPs at optical wavelengths (Seidel *et al.*, 2005). Later experiments (Noginov *et al.*, 2008a,b) also involving dye gain medium showed increased compensation of metal losses. More recently, quantum dots embedded in polymer were used

as a gain medium to increase SPP propagation length by about 30% (Bolger *et al.*, 2010) on a gold film.

So-called long-range SPPs consist of thin metal films bounded by symmetric dielectric layers. The attenuation of specific modes supported by these thin films is an order of magnitude smaller than that for single-interface SPPs; however, the confinement of the optical mode is poor (Dionne *et al.*, 2005; Prade *et al.*, 1991). Theoretical studies of long range SPPs have found gains required to overcome losses in semiconductor-clad silver films to be on the order of several hundred cm^{-1} or less (Nezhad *et al.*, 2004). The stimulated emission of long-range SPPs was first reported for a gold stripe embedded in Er-doped glass (Ambati *et al.*, 2008) in 2008. Since then, there have been several reports of amplification in long-range SPP waveguides, predominately employing dye gain medium (De Leon and Berini 2010; Gather *et al.*, 2010). The first demonstration of lasing for long-range SPPs was given recently for a thin gold film embedded in semiconductor gain medium and lasing at a wavelength of 1.46μm (Flynn *et al.*, 2011).

4.2. Metal-clad structures

Probably the greatest number of demonstrations of lasing in small metallic structures has been for metal-clad semiconductor devices. These devices perhaps have the greatest potential for confining light in small gain regions and also can be easily modified for electrical pumping. For long-term success, it is likely that the ability to electrically pump devices, and also offer a significant improvement in light confinement and integration density compared to dielectric lasers, will be key. A number of different forms of metal-clad lasers have been shown. Each of the major types will be treated in separate sections.

4.2.1. Pillar surface-emitting devices

The first metallic nanolaser demonstrated (Hill *et al.*, 2007) was a pillar type nanolaser. This first sort of device involved encapsulating a heterostructure pillar, which has a higher index in the center of the pillar (Fig. 9.3A). In the devices we have made, the lower index material consists of InP and the higher index InGaAs. The mode of interest which resonates in such a pillar has a frequency close to the cutoff frequency of the circular waveguide with the InGaAs core. Since the cutoff frequency of the waveguide above and below the InGaAs region is higher than the resonant frequency, the mode is trapped on the InGaAs region (see Fig. 9.3B). The modal energy in such a cutoff waveguide is actually bouncing back and forth between the sidewalls of pillar. This can be seen in the Fig. 9.3B, where the Poynting vector is shown. Due to the optical losses of the encapsulating metal, net energy flow is into the sidewalls of the pillar. However, because of the finite length of the bottom InP region in the

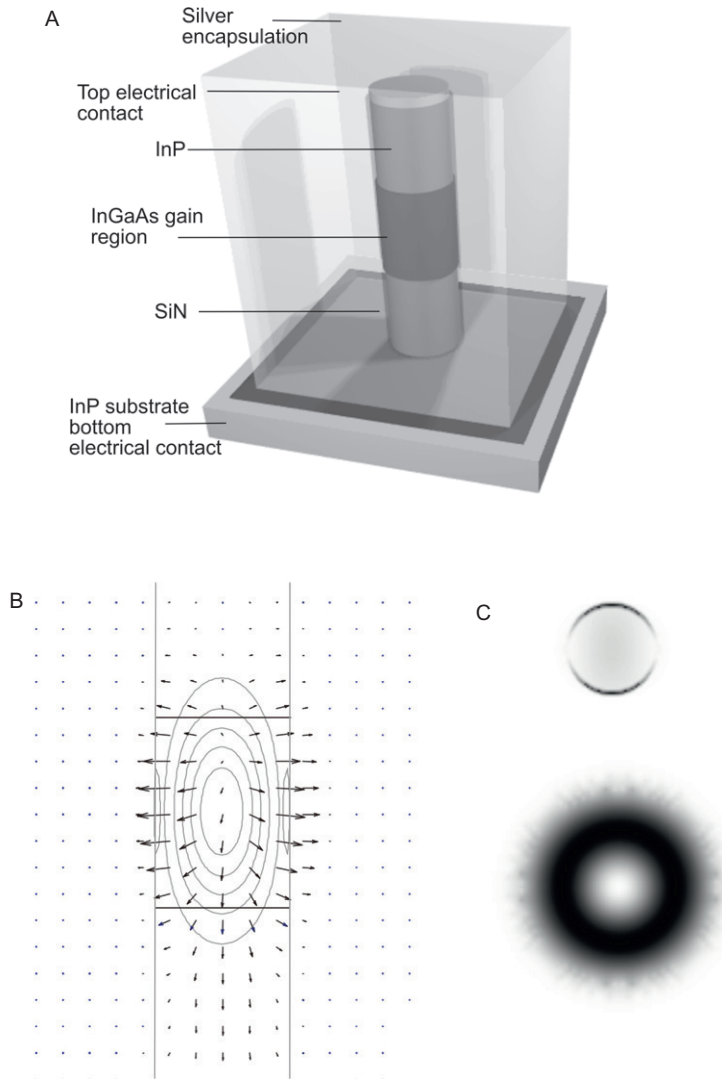

FIGURE 9.3 (A) One approach for metallic nanolasers with surface-emitting properties is to encapsulate a semiconductor heterostructure pillar in an insulator then a low-optical loss metal such as silver or aluminum. Such an approach is particularly suitable for electrical pumping of the laser. In the figure shown, an InP/InGaAs heterostructure is used with SiN insulator. Some light in the optical mode escapes through the bottom of the pillar and the substrate. (B) The optical mode in such structures is trapped on the InGaAs gain region in the center of the pillar due to refractive index differences. The contour lines show $|E|^2$ of the trapped optical mode in a slice through the pillar center, with color giving intensity. The arrows show the magnitude and direction of the time averaged Poynting vector for this slice of the mode and show that the energy of the mode is mostly being dissipated as heat in the metal sidewalls. (C) Plot of $|E|^2$ for top, a HE11 mode, and bottom a TE01 mode, showing a cross-section through the center of the pillar. Black indicates highest intensity. Note for the HE11 the intensity maximum is at the metal/dielectric interface, while for the TE01, there is modal minimum at this interface. Figure adapted from Hill (2010).

pillar, there is some coupling of the modal energy into the substrate below the pillar. The amount of power emitted into the substrate can be tuned by adjusting the amount of cutoff waveguide below the InGaAs, and this will be discussed in a later section. The light escaping from the aperture at the base of the pillar propagates with a component in the vertical direction, and hence, the device can be used as a form of surface-emitting laser.

By adjusting the size and shape of the cross-section of the pillar different resonant modes can be obtained. At present, perhaps the most interesting modes are the lower order modes of such cavities, for example, HE11 or TE01 modes (Hill *et al.*, 2007; Mizrahi *et al.*, 2008; Nezhad *et al.*, 2010), as these modes result in the smallest device and modal volumes. The benefits of small device size and modal volumes include high Purcell factors helping to reduce threshold and nonradiative losses, smaller active regions to reduce power and also improve prospects for heat sinking, and finally a large free spectral range to ensure single-mode operation.

The actual initial devices employed a HE11 mode which is the lowest-order oscillatory mode that can occur in such a device (Prade and Vinet, 1994). Such a device has a relatively low Q, 180 at RT for silver, though a good confinement of the optical mode on the gain region (~0.4). In theory laser operation at RT should be possible with a threshold current on the order of 30 μA. These initial devices used gold as the confining metal and only worked at cryogenic temperatures (77 K), with low-threshold currents on the order of 7 μA (Fig. 9.4). However, it has been shown that

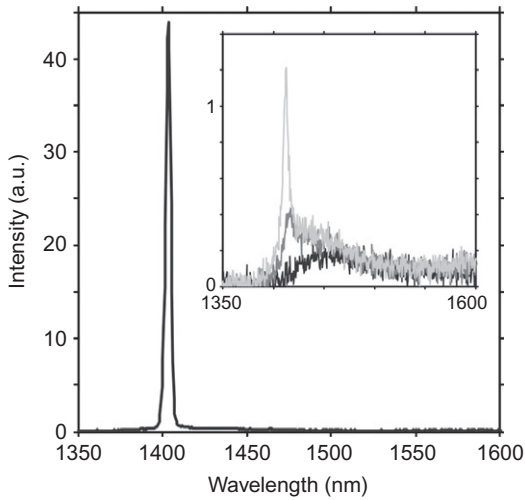

FIGURE 9.4 Above-threshold emission spectra for a HE11 mode pillar device from Hill *et al.* (2007) with a pump current of 60 μA at 77 K. Inset shows spectra around the lasing threshold: 3 (black), 5 (gray), and 7 (light gray) μA, all at 77 K.

moving to higher order modes by increasing the diameter of the pillar, much higher Qs can be obtained (Mizrahi *et al.*, 2008). In fact with an optimum choice of the dielectric region surrounding the semiconductor core, Qs in the region of several thousands can be reached. The high Q along with good modal overlap with the gain region, can lead to quite low-threshold gains, of the order of $100\,\mathrm{cm}^{-1}$ or less. Such devices have been shown to work optically pumped at RT (Nezhad *et al.*, 2010), and there is potential for RT electrically pumped versions to have microampere level threshold currents. It has been shown that without the metal confinement layer on these devices, both the Q and the modal overlap with the gain region are substantially reduced. Thus the presence of the metal is crucial to permit lasing (Nezhad *et al.*, 2010).

Larger pillar devices can exhibit a wide range of resonant modes, including whispering gallery-type modes, and other standing wave type modes not seen in similar size dielectric cavities. Generally, modes in these larger devices have high-quality factors. Importantly, these devices can provide electrically pumped lasers in planar technology that are smaller than is possible with microdisk devices and can be coupled to waveguides (Che and Huang, 2010; Che *et al.*, 2011a,b).

For use as a VCSEL replacement, both the device efficiency and shape of the output beam will be of importance. Studies have been performed on these aspects, and predictions of efficiencies in the order of 50% have been made (Huang *et al.*, 2010b). For the devices relying on trapped cutoff modes to obtain the vertical confinement, there is a tradeoff between the maximum cavity quality factor Q, and the amount of light emitted to the external environment, as in most laser devices (Chang *et al.*, 2010a). By making the length of the cutoff waveguide under the active layer shorter, more of the modal light can escape the cavity. Figure 9.5A shows the structure of a surface-emitting pillar device. This device operates with a TE01 resonant mode, a plot of which is given in Fig. 9.5B. Figure 9.5C shows a plot of the cavity Q for various lengths of the InP waveguide below the InGaAs gain region, h. The device has a circular center gain region of InGaAs 440 nm in diameter, and 300 nm thick, with a silicon dioxide insulation layer 80 nm thick. For a long InP waveguide section, the Q is approximately 1400. For an optimized choice of the insulation layer thickness, maximum Qs in the order of 3000 are possible (Nezhad *et al.*, 2010). For shorter and shorter sections of waveguide the Q decreases, indicating that more and more energy is escaping to the substrate.

For many VCSEL applications, it is likely that the divergence of the beam emitted from the base of the pillar should be small. It has been shown that the divergence of light exiting from a subwavelength hole can be controlled by patterning of the metal around it (Lezec *et al.*, 2002). Other methods to control the beam shape may be the use of tapering of the

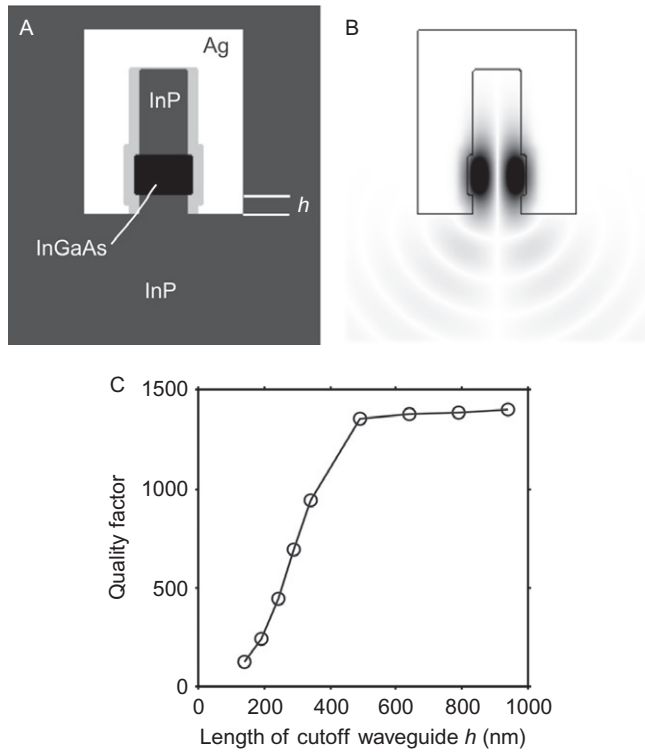

FIGURE 9.5 (A) Slice through silver-encapsulated semiconductor core pillar device, showing details of its structure used in a simulation. The height of the InGaAs core is 300 nm. The light gray region between the InGaAs core and silver is the SiO_2. The substrate below the pillar is InP. The height parameter h can be varied to modify the Q of the cavity, allowing more or less light from the cavity mode to leak to the outside of the cavity. Typically, electrical contacts to these pillar devices to pump the InGaAs gain region can be made through the top of the pillar via the actual silver encapsulation, and another contact to the other side of the InGaAs gain region via the InP substrate. (B) FDTD simulation results showing $|E|$ plot of a slice through the pillar, indicating a TE mode centered on the InGaAs and leaking power to the substrate. Black shows the highest intensity. (C) Plot of quality factor of cavity versus length of InP stub under the InGaAs. Shows trade offs can be made between Q and emission efficiency. Adapted from Hill (2010).

pillar structure below the active region. In this scheme, the pillar can be used to form a horn antenna (Hill and Marell, 2011; Silver, 1949).

Another concept in metallic surface-emitting devices has also been demonstrated recently (Lu and Chuang, 2011; Lu *et al.*, 2010, 2011a); see Fig. 9.6. Although similar to the concept presented in Fig. 9.3, in that both are round pillars containing heterostructures, there are a number of

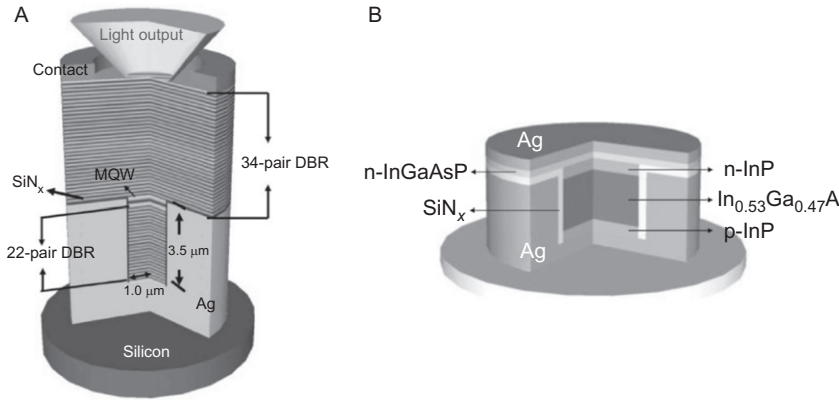

FIGURE 9.6 Another form of a pillar cavity that appears very similar to that of Fig. 9.3. However, here the mode propagates up and down in the pillar, and the resonant wavelength is always below the cutoff wavelength in the pillar waveguide (Lu and Chuang, 2011; Lu *et al*., 2011a,b). The mirror at the pillar top is formed by the silver contact. (A) In one case, the mirrors are formed by Bragg reflectors (possibly in combination with a silver layer), similar to a traditional VCSEL. (B) In another case, the mirrors are formed by a thin silver films, which also serve as electrical contacts. Figures taken from Lu *et al*. (2011a) and Lu and Chuang (2011).

fundamental differences. In particular, the device of Fig. 9.6 does not rely on a trapped cutoff mode in the center of the pillar. Rather, the resonant mode has a frequency above the cutoff frequency of the cylindrical metal waveguide. The mode is propagating up and down the waveguide. The resonator is formed by having mirrors at either end of the cylindrical waveguide. Typically, the top mirror is formed by the metal of the top contact. In the examples given in Lu *et al*. (2011a) and Lu and Chuang (2011), the bottom mirror can be formed by a Bragg grating or by a partially reflective metal mirror. This concept is closer to the original concept of a VCSEL, nanowire lasers, and also numerical studies of looking at lasing in metal-coated nanowires (Maslov and Ning, 2007). In this particular concept, the frequency of laser oscillation is determined by the length of the cavity in the vertical direction, in combination with any frequency selective mirrors that may be employed. Original VCSEL designs also incorporated metallic mirrors (Iga *et al*., 1988). However, the metallic propagating mode devices here also constrain the optical mode in the lateral direction, via the thick metallic waveguide. The lateral metallic confinement can lead to smaller size and better heatsinking compared to VCSELs (Lu *et al*., 2011b). There are a number of advantages and disadvantages of this second approach compared to the cutoff-mode devices discussed previously. For example, the propagation direction of the output light is automatically in the vertical direction, and the pillar

diameter and thus output aperture size are independent of the resonant wavelength. However, the wavelength can no longer be easily changed over a wide range via the pillar width.

4.2.2. Purcell factor

One of the interests in making lasers smaller is to increase the spontaneous emission rate and coupling to the lasing mode via the Purcell effect (Koenderink, 2010). To increase the Purcell factor (F_{cav}) and increase the spontaneous emission rate, one must increase the ratio of Q/V_{eff} for the cavity, where V_{eff} is the effective modal volume of the cavity. In dielectric cavities, V_{eff} has a minimum limit due to the diffraction limit, and the best way to increase F_{cav} is to increase the Q. Indeed, dielectric cavities can achieve Q factors on the order of 10^6; however in these cases, only emitters with wavelengths which overlap with the very narrow bandwidth of the cavity experience enhanced spontaneous emission. Metallic cavities have much lower Q factors, but V_{eff} can be much smaller, and impressive spontaneous emission enhancement can in theory be achieved over wide bandwidths (Hofmann *et al*., 2011). Most of the small metallic cavity lasers demonstrated show a significant enhancement of spontaneous emission into the lasing mode via the Purcell effect. For classical dielectric cavities V_{eff} is defined as:

$$V_{\text{eff}} \equiv \left[\int_V \varepsilon\left(\vec{r}\right)\left|\vec{E}\left(\vec{r}\right)\right|^2 \mathrm{d}^3\vec{r}\right] / \max\left[\varepsilon\left(\vec{r}\right)\left|\vec{E}\left(\vec{r}\right)\right|^2\right]$$

For metallic cavities, however, the energy density $\varepsilon\left(\vec{r}\right)\left|\vec{E}\left(\vec{r}\right)\right|^2$ that is in the mode volume needs to be defined correctly for parts of the mode occurring in the metal. The energy density in lossy dispersive media has been considered by a number of people (Landau and Lifshitz, 1960; Loudon, 1970). A recent review and comparison of the various approaches is given in Nunes *et al*. (2011). We employ the energy density definition given in Loudon (1970) (Eq. 9.7). For a dipole emitter at the spatial and spectral mode maximum of the cavity, and aligned with the mode field, F_{cav} is given by

$$F_{\text{cav}} \equiv \frac{3Q}{4\pi^2 V_{\text{eff}}}\left(\frac{\lambda}{n}\right)^3 \tag{9.12}$$

where λ is the resonant wavelength, and n the effective index of the cavity. In general, the spectral and spatial overlap of the emitters in the cavity has to be also taken into account when determining spontaneous emission rate. Furthermore, for cavities containing bulk semiconductor gain medium, emitters are distributed evenly over the gain medium. For this case, it can be useful to define a V_{ave}, similar to V_{eff}, but with the denominator of V_{eff} replaced by the

average value of $\varepsilon\left(\vec{r}\right)\left|\vec{E}\left(\vec{r}\right)\right|^2$ in the gain medium. However, V_{ave} is also not an ideal measure to calculate F_{cav} because it does not take into account carrier diffusion effects. The diffusion length (Fujita and Baba, 1999) of carriers in typical semiconductors at RT can be of the order of 1–2 μm, far greater than the distance between the minima and maxima of the modal field (~100 nm). The long diffusion length will result in carriers flowing from low recombination rate areas to high recombination rate areas at the field maximum. Hence, the actual F_{cav} will likely lie somewhere between the extremes predicted by V_{ave} and V_{eff}. In Hill *et al*. (2007), rate equation models are used which incorporate the cavity-enhanced spontaneous emission effects. Good agreement was obtained with the measured emission characteristics when using an F_{cav} of approximately 60, Fig. 9.7. Such values are typical of what is found in other small metallic laser demonstrations (Nezhad *et al*., 2010; Yu *et al*., 2010).

4.2.3. Technology

It is worthwhile to give some mention to a few of the technological issues behind metallic laser devices. Arguably, the most critical and difficult aspect of making metallic nanolasers, in particular if trying to obtain RT and electrically pumped operation, is the actual realization of the simulated devices. However, the technological issues involved in the

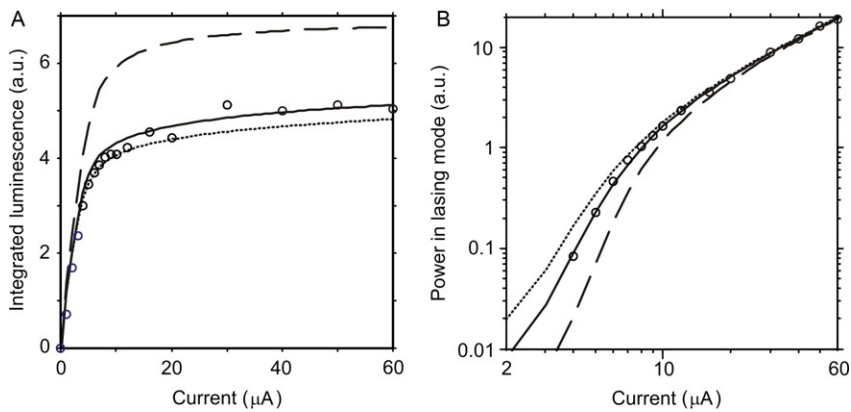

FIGURE 9.7 Comparison of a rate equation model predictions to 77 K measurements of a HE11 mode pillar device from Hill *et al*. (2007), showing the importance of the Purcell effect. (A) Plot of measured integrated luminescence and (B) lasing mode power. The solid lines show a rate equation model fit to the experimental data (circles), for various values of F_{cav}: solid line, 60; dotted lines, 150; dashed line, 17. The F_{cav}=60 lines were scaled in the vertical direction to match at one point of the measurement data. The other lines were scaled equally. The lasing mode power is shown on a logarithmic plot to better show the fit at small powers. Figure adapted from Hill *et al*. (2007).

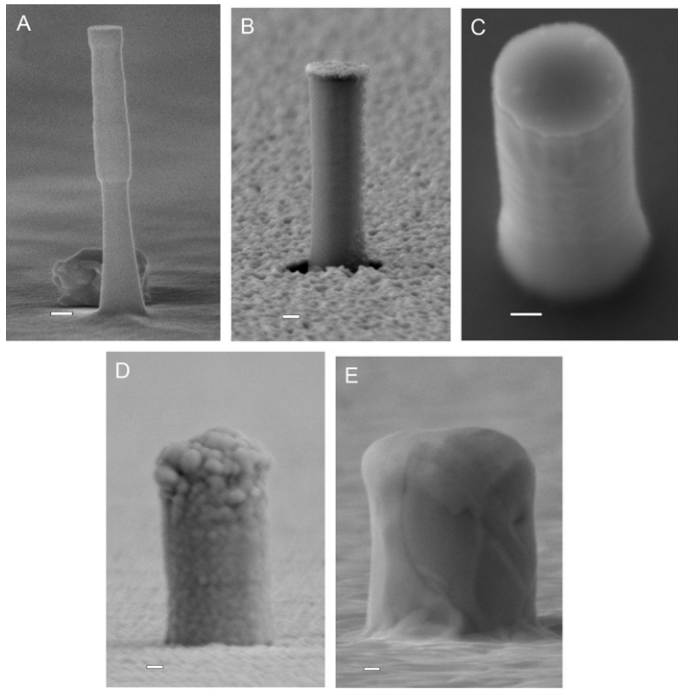

FIGURE 9.8 (A) Scanning electron microscope (SEM) image of an etched InP/InGaAs heterostructure pillar. The scale bars in all images represent 100nm. (B) SEM image of a pillar encapsulated in SiN and with a Ti/Pt/Au n-contact at the top of the pillar, and Ti/Au layers around the base. Note how the sidewalls of the pillar are free of high-optical loss metal. (C) SEM image of a pillar coated with SiN, and the SiN has been removed from just the top of the pillar by resist planarization and reactive ion etching for SiN on the exposed top of the pillar. (D) SEM image showing silver evaporated around a pillar. (E) SEM image of silver on pillar after being annealed at 400°C for 60s. Note the large grain structure.

realization will likely be specific to a particular concept and also a particular gain material. Here, a brief description of some of the issues involved with the manufacture of the pillar and waveguide devices, for InGaAs gain material are discussed. It is hoped that some of the issues discussed will be applicable to other materials systems and nanolaser concepts. Figure 9.8 shows some examples of the technology issues mentioned here.

4.2.3.1. Pillar etching and surface recombination Most of the pillar or waveguide devices shown thus far have the semiconductor core formed by dry etching an epitaxially grown wafer. The pattern of the pillar cross-section is written on the semiconductor surface; then typically reactive ion etching (RIE) is used to transfer that pattern into the semiconductor. The first main issue is that the Q and localization of the mode in the pillar is

strongly dependant on the sidewall shape. A deviation of even just 1° from a vertical sidewall can significantly spoil the cavity Q. So well-controlled isotropic dry etching is required, such as with ICP (inductively coupled plasma) RIE. A second major issue is the damage done by the etching process to the semiconductor surface. Damage can cause defects in the semiconductor crystal lattice, which are sites for nonradiative carrier recombination. Typically, this damage to the sidewall can be eliminated by removing the damaged material after etching. In Hill *et al.* (2007) and Yu *et al.* (2010), this damage removal is achieved by oxidizing the first couple of nanometers of the semiconductor surface, then removing the oxidized surface with an acid. Each time the process of oxidization and oxide removal is repeated, a few nanometers from the surface are removed. In this way, there is a precise and controlled removal of damaged material. Typically, only a few tens of nanometers need be removed. In Wang *et al.* (2011b), it is shown that with appropriate dry etching and sidewall damage removal, high-quality InGaAs/InP nanowire pillars can be made down to remarkably small diameters of approximately 20nm.

4.2.3.2. Dielectric layer The conformal coating of the pillar with a dielectric layer is a particularly critical step. For TM or plasmon modes, it is desirable to have the dielectric layer as thin as possible and also with a high-refractive index to minimize the energy contained in it. Additionally, the dielectric layer also must be sufficiently thick to not breakdown when a voltage is applied across the laser diode. For TE modes, the dielectric layer can be thicker (Mizrahi *et al.*, 2008). The dielectric must not cause damage to the semiconductor surfaces when it is deposited and finally needs to afford protection to the semiconductor surface during subsequent cleaning and deposition steps in the device manufacture. To achieve these different tasks in Hill *et al.* (2007), the dielectric layer consisted of a number of layers of silicon nitride, deposited at various temperatures (Kim *et al.*, 2005).

4.2.3.3. Metal layers The most critical metal layer is the low-optical loss metal which is in contact with the cavity mode. This needs to be of high purity with a good crystal structure as mentioned in Section 2. Unfortunately, the most common low-optical loss metals, gold and silver, typically exhibit poor adhesion to most dielectrics. Often a thin layer of another metal such as titanium (Lakhani *et al.*, 2011; Yu *et al.*, 2010) is used to improve the adhesion. However, this adhesion layer greatly increases the optical loss. In Hill *et al.* (2009), the approach taken was to place a gold/titanium layer around the base of the pillar (Fig. 9.8). After the silver was deposited on the pillar sidewall and base, the silver was annealed at 400°C for 60s, to obtain a large grain size. The annealing also caused the gold to dissolve in the silver, which bonded the silver to the substrate via the titanium layer at the base of the pillar, but avoided loss-inducing titanium close to the optical

mode. Another critical issue is to make a low resistance contact to the top of the pillar. In Hill *et al.* (2007), the silicon nitride dielectric was opened just at the top of the pillar, by planarization with photoresist and etching back with developer to expose just the pillar top. Then the dielectric at the top was removed with dry etching. Further resist planarization was used to expose the open pillar top and deposit via evaporation thin Ti/Pt/Au layers (Shantharama *et al.*, 1990). Liftoff in acetone removed the contact metals from all but the pillar tops (Fig. 9.8).

4.2.4. Metal insulator–metal waveguide structures

The surface-emitting devices discussed above will most likely exploit higher Q oscillatory modes inside the metal cavities (Prade and Vinet, 1994). These modes have minimum sizes close to the diffraction limit, ($\lambda/2n$). Uniquely, metal cavities can confine light to regions smaller than the diffraction limit. The high intensity of the electric field that occurs at a single metal–dielectric interface as shown in Section 2 can lead to a modal volume V_{eff} smaller than the diffraction limit (Barnes *et al.*, 2003), particularly when the resonant frequency approaches the metal plasma resonance ω_p. However, the optical field still extends distances on the order of a wavelength away from the interface, especially for longer wavelengths, placing a limit on how closely devices can be packed. As mentioned in Section 2 and Fig. 9.1B, one of the few metallic structures that permit true deep subwavelength confinement of light is the MIM waveguide structure (Dionne *et al.*, 2006; Prade *et al.*, 1991). The MIM waveguide can confine light inside an arbitrarily small insulator layer between the two metal slabs. Penetration into the metal on each side of the insulator is typically also limited to a few tens of nanometers (Dionne *et al.*, 2006), allowing in principle tightly packed waveguides (Zia *et al.*, 2004).

A number of groups have performed experiments involving placing optical emission and gain material inside MIM waveguide structures. The most obvious method to make MIM waveguides is to deposit metal then insulator then metal onto a flat substrate. This construction method has been used to make surface plasmon-emitting devices (Koller *et al.*, 2008; Walters *et al.*, 2009), where the insulator between the metals has been replaced by light-emitting material. This construction technique has also been successful in making lasing devices (Walther *et al.*, 2010) with semiconductor gain material for far infrared wavelengths. In all these devices, the confining metal plates also serve as electrical contacts. For far infrared devices, the semiconductor layer thickness is several microns, permitting the use of specially doped layers to give efficient electrical contacts. However, for shorter wavelengths, where the semiconductor layer thickness is reduced to a few tens of nanometers, providing both good contact layers and gain layers may be difficult.

Another approach has been to place the MIM waveguide on its side, by etching long thin waveguide structures through the epitaxially grown substrate. Then evaporate metal onto the sidewalls of the pillar. The refractive index difference between the InP and InGaAs isolates the mode on the InGaAs gain region (Kusunoki *et al.*, 2005). The advantage of this configuration is that the electrical contacts which inject the carriers into the gain InGaAs region are located away from where the tightly confined optical mode is. Furthermore, a thin insulation layer isolates the metal from the semiconductor gain medium (Fig. 9.9A). This waveguide concept was also examined theoretically in Chen *et al.* (2010), though after they had already been demonstrated (Hill *et al.*, 2009).

Sections of these waveguides terminated in metal mirrors to form Fabry–Perot cavities were shown in Hill *et al.* (2009). These cavities were realized by simply totally encapsulating a pillar which has a thin rectangular cross-section in silver. The dielectric and silver layer thickness was the same all round the pillar. Some light from the lasing mode could escape through the substrate, to show what is occurring inside the cavity. For improved light extraction, the waveguide can be cut to remove the silver encapsulation at the end of the cavity. With this concept, we have shown lasing based on the propagation of TM_0 or gap-plasmon modes along the waveguide (Hill *et al.*, 2009). The width of the semiconductor core in these waveguides was as thin as $\sim$90nm. Electrical contacting to such thin waveguides is possible because the small electrical contact at the top of the semiconductor core is connected to a much larger metallic structure. The larger metallic structure includes the encapsulating silver shell (Fig. 9.9).

A number of other forms of cavity can be created using such a waveguide concept. Small ring lasers were proposed in Chen *et al.* (2010) and Kim and Ku (2011a,b), and actually, the smallest ring lasers ever made were demonstrated recently in Kim and Ku (2011b). Such ring lasers can have a number of advantages over pillar lasers above in that by varying the waveguide thickness, the wavelength can be tuned, even though the laser dimensions are kept constant (Kim and Ku, 2011a,b). More recently, distributed feedback via Bragg gratings has been introduced into MIM waveguides to create single-mode laser cavities (Marell *et al.*, 2011). Such Bragg gratings can be easily introduced into the waveguide structure by simply modulating the width of the semiconductor core during lithography at the beginning of manufacture. A scanning electron micrograph of such a modulated core waveguide is given in Fig. 9.10. These metallic Bragg gratings offer unique properties such as extremely high-reflection coefficients, greater than $5000\,cm^{-1}$, which is an order of magnitude higher than for dielectric systems.

Recently, it has also been shown that even without a heterostructure in the waveguide it is possible to obtain lasing (Wang *et al.*, 2011a). In this

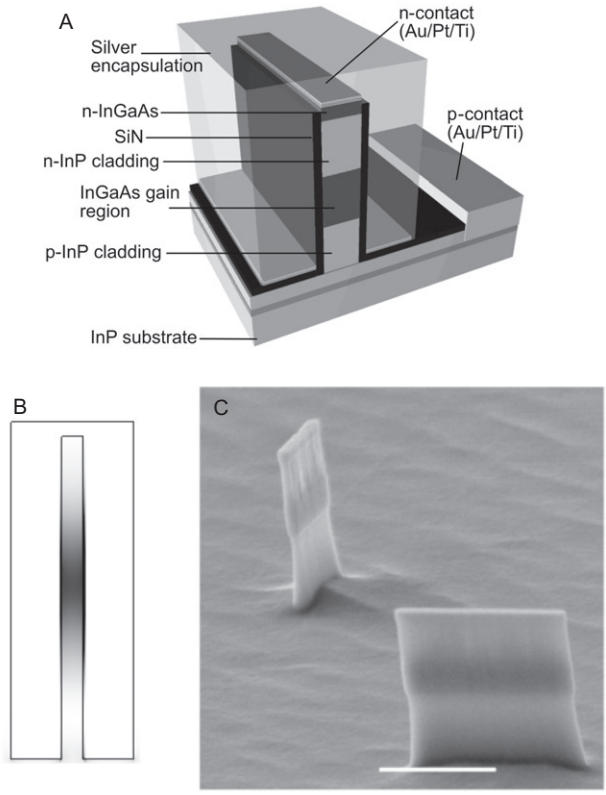

FIGURE 9.9 (A) Electrically pumped MIM waveguide structures which has the usual flat MIM configuration turned on its side. The propagating mode is confined to the InGaAs gain region in the center of the waveguide by index differences. The light gray layers to the side and at the bottom of the ridge are Au/Ti layers, employed to help bond the silver encapsulation to the semiconductor/dielectric core. The schematic shows a cut through the ridge structure. In actual devices, the ends of the ridge are also encapsulated in dielectric and silver of the same thickness as the sidewalls. Adapted from Hill *et al.* (2009). (B) Plot of $|E|^2$ for the gap-plasmon mode taken horizontally across the waveguide structure, showing mode localized in the center of the pillar. Black shows highest intensity. (C) SEM photos of sections of waveguide cores, which after being encapsulated in silver will form Fabry–Perot cavities. The scale bar is 1μm.

experiment, GaN ridges were encapsulated in aluminum. The presence of the metal was able to offer the increase in quality factor and modal confinement needed for lasing. Importantly, lasing occurred at ultraviolet wavelengths and RT.

Another, closely related MIM struture that has received attention is the nano-patch laser. This is a small MIM structure that is placed on a large

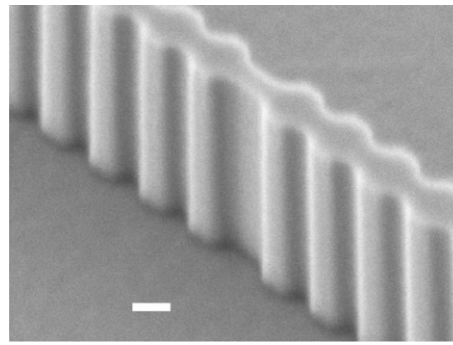

FIGURE 9.10 Semiconductor core of MIM waveguide with modulated width used to form plasmonic DFB lasers as reported in Marell *et al.* (2011). The scale bar is 100 nm.

flat gold surface (Manolatou and Rana, 2008; Nagpal *et al.*, 2009). The structures are related to microwave-patch antennas (Manolatou and Rana, 2008). These devices do not support SP modes, but rather either TE or TM oscillatory modes between the two plates. In theory, such devices have been studied and shown to have low-threshold currents of a few microamperes, and useful and controllable radiation patterns. More recent work has also shown that with optimization of the dielectric thickness in the structures, high Q and low-threshold gains are possible, even at RT (Ding *et al.*, 2011a).

In most of the MIM structures shown, and in particular those that are electrically pumped, the gain medium core is surrounded by a thin insulator (more correctly a MISIM, metal insulator semiconductor insulator–metal waveguide). The insulator surrounding the semiconductor typically has a lower refractive index, n, than the semiconductor. For example, InGaAs with $n=3.6$ and silicon nitride with $n=2$. The discontinuity in the refractive index of the MISIM waveguide core causes a significant deviation from the mode shape of a TM_0 mode (Prade *et al.*, 1991; Fig. 9.11). However, as with homogeneous core MIM waveguides, the insulator part of the waveguide can be made arbitrarily thin while still propagating a mode. One feature of the MISIM mode is that the electric field in the thin insulator region is much higher than in the semiconductor region. This leads to a very small modal volume if the standard definition of modal volume is used. A very similar behavior occurs for the single metal interface, with a low refractive index dielectric placed between the metal and semiconductor (Oulton *et al.*, 2008). As mentioned in Section 2, the propagation length of the SPs in such systems is increased. However, the ratio of modal energy in the semiconductor to that in the metal decrease, thus requiring higher gain for lasing (Chen *et al.*, 2010; Hill, 2009). For plasmon-mode MIM devices, the dielectric layers should be

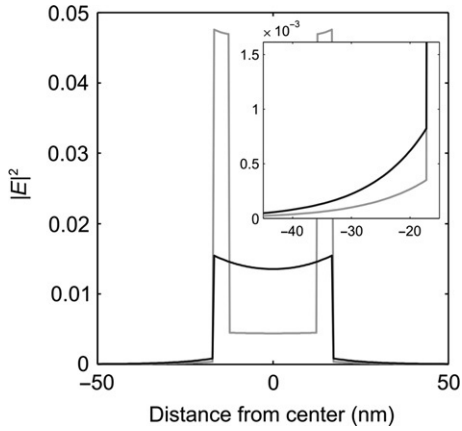

FIGURE 9.11 Plot of $|E|^2$ for the gap-plasmon mode taken horizontally across the waveguide structure for a 25-nm-wide InGaAs region and 5-nm-thick SiN insulator. Gray is for the real refractive indices of InGaAs and SiN, black when the SiN has the refractive index equal to InGaAs. A significant proportion of the modal energy can travel in the insulator, which can increase the gain requirements from the InGaAs. Inset shows detail of the mode tail in the metal. It can be clearly seen that the low-index dielectric case has less energy in the metal. Adapted from Hill (2010).

made as thin as possible and with as high a refractive index as possible, unless the strong electric field in this layer is to be exploited in some manner.

Another interesting aspect that has been observed in a number of experiments with metallic waveguide devices (Hill *et al.*, 2009; Lu *et al.*, 2009; Oulton *et al.*, 2009) is that the group index exhibited in these waveguides is much higher than typically seen in conventional dielectric devices. In fact, group indices of 10 or higher have been reported. The current belief is that the high gain (in the order of several thousand cm^{-1}) required in the semiconductor core also causes a high dispersion in the semiconductor. The connection between gain and dispersion can be seen in Fig. 9.2, for gain medium with a Lorentzian gain profile. Although the actual dispersion in semiconductor material is more complex (Bennett *et al.*, 1990), the general concept applies. Even though the higher dispersion results in higher energy storage in the gain medium, the device threshold gain is independent of the gain medium dispersion, given the assumptions taken in Section 2.

Thus far, in the vertical direction the mode in the MISIM waveguide is confined in the center by the increased refractive index of the gain region. Effective index arguments have been used to give an explanation of this behavior (Kusunoki *et al.*, 2005). For the actual MISIM waveguide, care needs to be taken in applying effective index arguments, as the large

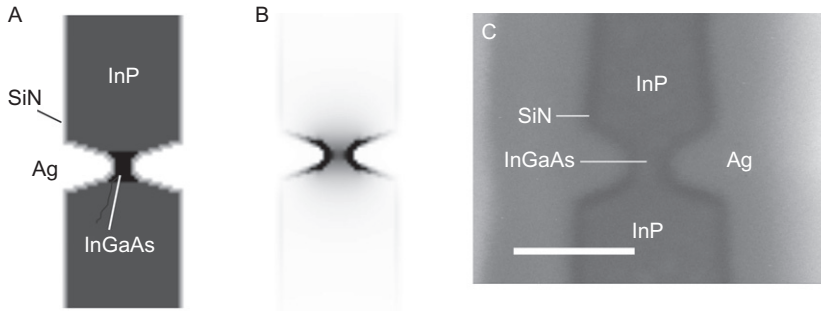

FIGURE 9.12 (A) Structure of an active surface plasmon polariton gap waveguide. Lithography, dry etching, and selective wet etching can be used to form the three-dimensional nanostructure. Slice through simulated 3D structure, with deviations from the idealized shape to take into account what can be achieved with typical fabrication techniques. The InGaAs is 45nm high and 25nm wide. The InP cladding has an indentation of approximately 60nm on each side. (B) Plot of $|E|^2$ from FDTD simulation of such a structure, showing tightly confined mode. Black is highest intensity. (C) Cross-section of a completed waveguide which has been encapsulated in silver. The scale bar is 100nm. Adapted from Hill (2010).

proportion of modal energy is in the low-index insulator. To provide a stronger confinement in the center of the MISIM waveguide, indentation of the waveguide sidewalls can be combined with the index change (Kusunoki *et al.*, 2005; Tanaka and Tanaka, 2003), as shown in Fig. 9.12. Effective index arguments do not explain well the mode behavior. Furthermore, with the indented structures there are coupled-surface plasmon modes on the tops and bottoms of the metal indentations. Nevertheless, numerical simulations of such structures show that still the mode can be strongly confined in the vertical direction, even to levels well below the diffraction limit.

Figure 9.12A shows a slice through a simulated 3D structure of such a waveguide. Here the InGaAs region in the center is approximately 25nm thick and the InP cladding is indented approximately 60nm on each side. The SiN layer is 5nm thick all over the sidewalls. The grid size used in the simulation is 5nm, and this grid discretization can be seen in Fig. 9.12A. Figure 9.12B shows the mode profile of such a waveguide, calculated with 3D FDTD, for wavelengths of ~1500nm. It can be seen that in the vertical direction, the mode is tightly contained in the center region.

To place the minimum requirements on the optical gain medium requires that the optical mode energy to have the highest overlap with the gain medium. As can be seen from Fig. 9.12B, a significant amount of modal energy is contained in the dielectric layer between the semiconductor and the metal. Given the finite maximum gain available from any

optical gain material, then this reduced overlap due to the mode energy in the insulator and the metal will place a limit on the smallest size of device.

Calculations indicate that with widths of semiconductor around 25nm, an insulator thickness of 5nm, silver as the metal, and wavelengths around 1.5μm, then an optical gain of $\sim 4000 \text{cm}^{-1}$ is required (Hill, 2010). Such gains are in theory possible from bulk semiconductor materials, even at RT (Chuang, 2009). Higher optical gains in semiconductors have been inferred in recent nanolaser experiments (Gargas *et al.*, 2010; Lu *et al.*, 2010) involving semiconductors. If the miniaturization of the gain medium can be made to the point where quantum confinement effects occur, then potentially higher optical gains could be achieved on the order of 10^4 to 10^5cm^{-1} (Asada *et al.*, 1986). However, these very small devices require quite high gains and it may be that other approaches will be required to produce useful devices. While lasing has not yet been shown in these devices, it has been shown that it is possible in principle to manufacture such structures and still have working electrically pumped gain medium (Hill, 2010).

If MIM devices are to be of use in actual systems, then they will likely have to be coupled to either conventional dielectric or plasmonic passive waveguides. Fortunately, it has been shown in theory that indeed it is possible to couple plasmons in MIM waveguides with high efficiency to photons propagating in conventional dielectric waveguides (Ginzburg *et al.*, 2006). Furthermore, the conversion can be performed in a compact device. Such conversion is an important point for the deployment of plasmonic nanolasers, as signals from the lasers will eventually need to be transported over distances of at least several millimeters and the best way to do this is with dielectric waveguides or possibly waveguides supporting long-range SPs (Barnes *et al.*, 2003).

For short distances, MIM waveguides may also be used to transmit signals from nanolasers. In this case, it has been shown that it is feasible to use MIM waveguides to guide light around bends and split or combine it into multiple waveguides (Tanaka *et al.*, 2005).

4.3. Single metal–dielectric interface nanolaser structures

The previous laser devices have been based on structures which are enclosed on multiple sides by metal. It is also possible to create small lasers that have only a single metal–dielectric interface. Such cavities are formed by locally loading the metal/dielectric interface with a higher refractive index material. A number of different configurations have been used to form the cavity and confine the light in the high-index material region. The various approaches are summarized in Fig. 9.13.

The first approach demonstrated was to place a nanowire on top of a silver surface coated with a low refractive index dielectric (Oulton *et al.*, 2009; Fig. 9.13A). The presence of the nanowire forms a waveguide along

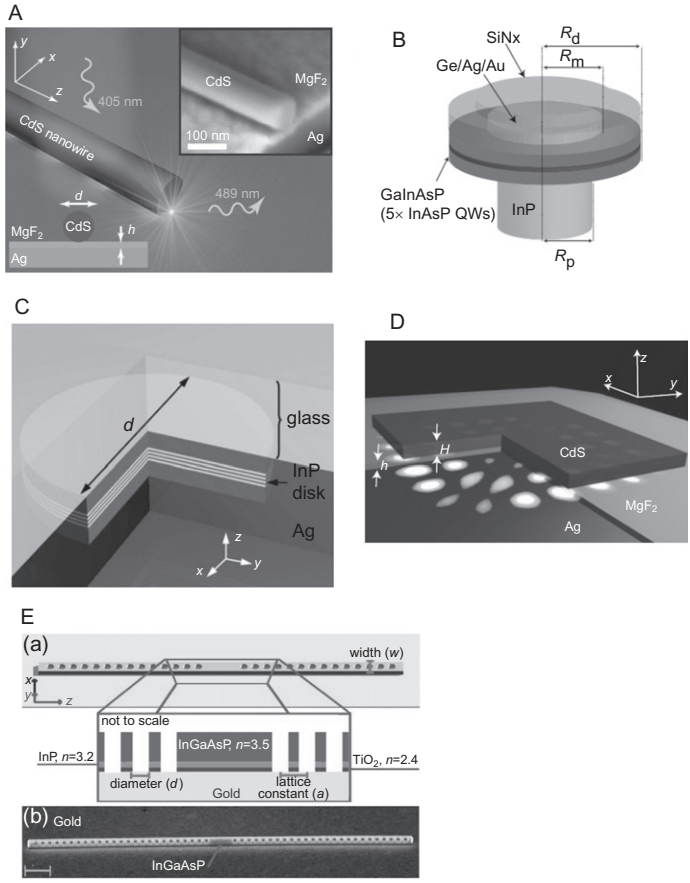

FIGURE 9.13 Various single metal/dielectric interface small plasmon-mode lasers, all of which are optically pumped. (A) Structure of nanowire laser which forms a highly localized hybrid plasmon mode in the thin dielectric layer where the nanowire is closest to the silver (Oulton *et al.*, 2009). The nanowire forms a Fabry–Perot cavity with the mode running along the length of the nanowire. (B) A microdisk coated with silver (Perahia *et al.*, 2009). At the silver/semiconductor interface surface plasmon modes occur and circulate at the disk edge as whispering gallery modes. (C) A so-called nano-pan laser (Kwon *et al.*, 2010), which consists of the semiconductor disk set into the silver. This cavity also has whispering gallery-type plasmon modes, but with stronger confinement than in Perahia *et al.* (2009). (D) Another whispering gallery-mode plasmon laser (Ma *et al.*, 2011), with a hybrid plasmon mode similar to Oulton *et al.* (2009). (E) An example of a plasmonic photonic crystal structure (Lakhani *et al.*, 2011). The dielectric loaded gold surface is modulated to form a bandgap for plasmons traveling along the metal/dielectric interface. Defects in the modulated structure can create plasmonic cavities.

the nanowire with a strong peak in the mode occurring in the low refractive index dielectric (Oulton *et al.*, 2008). The modal peak in the low-index dielectric is strongly localized in two dimensions. The reflections at the end of the nanowire helped form a Fabry–Perot cavity and were sufficient to obtain lasing in nanowires approximately 10 μm long. Another approach was to place metal on small disk of semiconductor (Fig. 9.13B). Here the SPPs can circulate around the disk in a so-called whispering gallery mode (Perahia *et al.*, 2009). A somewhat related approach but with stronger confinement and smaller size is shown in Fig. 9.13C. Here the high-refractive index material is set into the silver, to form a so-called nano-pan cavity (Kwon *et al.*, 2010). The small metallic sidewall formed around the semiconductor disk forms a stronger confinement for the whispering gallery SPP mode than for the open disk of Fig. 9.13B.

A final whispering gallery-mode device is shown in Ma *et al.* (2011; Fig. 9.11D). In this case, instead of a nanowire, a square patch of semiconductor, approximately $1\,\mu m \times 1\,\mu m$, is placed on a silver and dielectric substrate. Again the mode is highly localized in the low-index dielectric material.

Another approach is to use periodic perturbations to form a transmission bandgap over the metal surface (Barnes *et al.*, 2003). In the actual laser demonstration, higher index semiconductor material is perforated with holes and placed on a gold substrate to form a so-called plasmonic photonic crystal (Lakhani *et al.*, 2011). Such hybrid structures can combine the benefits of photonic crystal cavities with the heat sinking and electrical contacting of metals. It has been shown in theory that such devices based on 2D photonic crystal structures can be efficient light emitters (Kim *et al.*, 2009). However, the first of these hybrid plasmonic, photonic crystal structures shown to lase, was based on a nano-beam cavity placed on top of a metal substrate (Lakhani *et al.*, 2011).

4.4. The SPASER

Until now we have looked mostly at propagating surface plasmon modes (Hill *et al.*, 2009; Oulton *et al.*, 2009) or oscillatory modes contained by strong metal mirrors (Hill *et al.*, 2007; Nezhad *et al.*, 2010). Typically, the longest dimension of the cavity has been one-half wavelength or more. Small deep subwavelength metallic particles or corrugated metallic surfaces can exhibit highly confined plasmonic modes, particularly when they are resonant near the plasma wavelength of the metal. In these nonpropagating modes of small nanoparticles, the quasistatic approximation for Maxwell's equations is valid and often employed for mathematical simplicity (Wang and Ron Shen, 2006). For such small devices with poor coupling to propagating optical modes, the term SPASER (SP

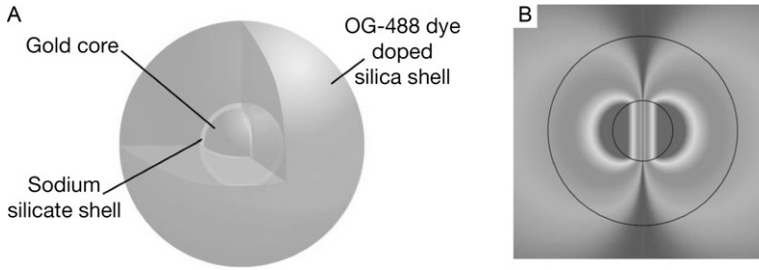

FIGURE 9.14 The smallest metallic nanolaser thus far demonstrated (Noginov *et al.*, 2009). (A) It consists of a gold nanoparticle 14 nm in diameter, encapsulated in a dye-filled sphere 44 nm in diameter. The structure is pumped with strong optical pulses and functions as a SPASER at green light wavelengths. (B) Plot of the electric field of the resonant plasmonic mode for the nanoparticle cavity.

amplification and stimulation emission of radiation) (Bergman and Stockman, 2003) has been coined. The first example of a SPASER device with subwavelength confinement of light in all three dimensions was demonstrated in 2009 (Noginov *et al.*, 2009). A schematic of the device is shown in Fig. 9.14. It consists of a gold nanoparticle sphere approximately 14 nm in diameter, surrounded by a silica shell doped with a dye gain medium, giving a total device diameter or 44 nm. A large number of such devices were manufactured by chemical means and placed in suspension in water. The solution of nanospheres was excited by strong pulses of light at wavelength of 488 nm and the appearance of a peak with narrowing linewidth was seen. These results were interpreted as showing SPASER action. However, individual isolated nanosphere devices have until now not been shown operating as SPASERs. This would be a technically challenging experiment but possible using, for example, scanning near-field microscope such as SNOM (Heinzelmann and Pohl, 1994).

A number of articles have calculated the mode profile for such a nanoparticle SPASER and also the gain required to compensate the losses of the metal nanoparticle (Avrutsky, 2004; Li and Yu, 2010; Noginov *et al.*, 2009). Typical estimates of the material gain required are in the range of 10^5cm^{-1}. This is an extremely high material gain. However, in theory given an optical cross-section for the dye molecules of $2.55 \times 10^{-16} \text{cm}^2$, and a packing density of 4.6×10^{20} dye molecules per cm^3, such optical gain could indeed be possible.

Some related concepts on the coupling of emission form quantum dots to nanoparticles have also been published (Protsenko *et al.*, 2005; Rosenthal and Ghannam, 2009). Some initial experiments in this field have already been carried out by coupling quantum dots to indium nanocrystals (Urbanczyk *et al.*, 2010). These experiments show enhanced spontaneous emission but not spaser operation.

5. FUTURE DIRECTIONS AND CONCLUSION

There has been considerable progress in the field of metallic nanolasers; however, there are significant important aspects that have yet to be properly explored. One aspect is the intrinsic modulation speed of the devices. There have been some predictions on this aspect (Genov *et al.*, 2011; Lau *et al.*, 2009; Stockman, 2010, 2011). Lau *et al.* (2009) predict that the electrical modulation bandwidth of small devices will be limited and that such devices can actually work faster as light-emitting diodes. However, Stockman (2010) and Genov *et al.* (2011) predict THz intrinsic optical modulation bandwidths for small laser devices. Measurements have yet to be made to confirm these predictions.

A significant motivation for developing metallic nanolasers is the improved heatsinking of the device afforded by the encapsulation of the device by metal. It is expected that improved heat sinking will allow much higher pump densities and hence higher speed devices. Indeed, pump current densities approaching the MA/cm^2 range have already been reported for continuous wave (CW) operation at cryogenic temperatures and pulsed operation at RT (Hill *et al.*, 2007, 2009). Furthermore, the devices should have a better ability to work in higher temperature environments. There does not appear to have been any simulation studies published of the thermal advantages. However, there has been some experimental studies of metal-encapsulated devices (Chang *et al.*, 2010a,b,c; Lu *et al.*, 2011b). Although the tested devices were still relatively large in size, they did show significantly improved thermal performance compared to dielectric cavity devices. In the future, it will be interesting to see how significant the heatsinking advantage for the metallic devices becomes.

For the long-term growth and success of the field, it is important that RT operation of CW electrically pumped metallic nanolasers is achieved, with an acceptable efficiency in the plasmon or light generation. Electrical pumping is simply the best way to achieve efficient plasmon generation with low power and subwavelength device size and pitch. Without electrically pumped nanolasers, probably the most efficient way to generate high-intensity localized fields is using some form of plasmonic taper to concentrate light from a conventional laser source. Some micron scale electrically pumped metal-coated lasers already work CW at RT (Lu *et al.*, 2011a,b). Other smaller devices are approaching RT operation (Ding *et al.*, 2011a,b). However, the performance of the devices is still far from what theory predicts. It is likely in the near future significant improvements in RT operation can be made as the manufacturing technology improves.

Most small metallic laser demonstrations thus far have been in the wavelength ranges spanning the near infrared to the ultraviolet. For the

infrared range longer than 2μm in wavelength, there has not been much work done. In this wavelength range, the metal losses can be considerably less than at shorter wavelengths. It may be that some of the metallic nanolaser design concepts will be applicable for small low-power light sources in this mid infrared wavelength region and offer some benefits in power and size compared to conventional laser designs.

Plasmonics is increasing as a research field and it appears that it will also become an important topic for industry (Schuller *et al.*, 2010; Stockman, 2011). Uniquely, plasmonics allow subwavelength devices with dense-packing densities. However, to permit complex systems to be made from plasmonic devices some means of signal amplification, and signal generation is required. Electrically pumped plasmon-mode amplifiers and lasers are the most obvious choice to fulfill these requirements and achieve small size and operating power. Furthermore, there is a perceived need for small, low-power and fast lasers for optical communications to be implemented down to the integrated circuit scale (Miller, 2009). In theory, metallic nanolasers are possibly the best option for this application. Although current performance of devices still falls well short of what can be expected, performance should improve toward predictions as manufacturing technology is developed. Furthermore, for the most tightly confined plasmonic devices, new materials or concepts may be found which will make their implementation easier.

As the technology for metallic nanolasers starts to mature, it is likely that new applications will emerge that profit from their unique characteristics.

REFERENCES

Albrecht, G. F., Eggleston, J. M., and Ewing, J. J. (1985). *Opt. Commun.* **52,** 401–404.

Ambati, M., Nam, S. H., Ulin-Avila, E., Genov, D. A., Bartal, G., and Zhang, X. (2008). *Nano Lett. B* **8,** 3998–4001.

Asada, M., Miyamoto, Y., and Suematsu, Y. (1986). *IEEE J. Quantum Electron.* **QE-22,** 1915–1921.

Atwater, H. A. (2007). *Sci. Am.* **296,** 38–45.

Avrutsky, I. (2004). *Phys. Rev. B* **70,** 155416.

Barnes, W. L., Dereux, A., and Ebbesen, T. W. (2003). *Nature* **424,** 824–830.

Bennett, B. R., Soref, R. A., and Del Alamo, J. A. (1990). *IEEE J. Quantum Electron.* **26,** 113–122.

Bergman, D. J., and Stockman, M. I. (2003). *Phys. Rev. Lett.* **90,** 027402.

Bolger, P. M., Dickson, W., Krasavin, A. V., Liebscher, L., Hickey, S. G., Skryabin, D. V., and Zayats, A. V. (2010). *Opt. Lett.* **35,** 1197–1199.

Chang, S.-W., and Chuang, S. L. (2009). *IEEE J. Quantum Electron.* **45,** 1004–1013.

Chang, S.-W., Lin, T.-R., and Chuang, S. L. (2010a). *Opt. Expr.* **18,** 15039.

Chang, S.-W., Ni, C. Y. A., and Chuang, S. L. (2010b). *Opt. Expr.* **16,** 10580–10595.

Chang, G.-E., Lu, C.-Y., Yang, S.-H., and Chuang, S. L. (2010c). *Opt. Lett.* **35,** 2373–2375.

Che, K.-J., and Huang, Y.-Z. (2010). *J. Appl. Phys.* **107,** 113103.

Che, K.-J., Huang, Y.-Z., Xu, H.-Y., and Cai, Z.-P. (2011a). *Opt. Lett.* **36,** 1374–1376.

Che, K.-J., Huang, Y.-Z., Chen, L.-J., Cai, Z.-P., and Xu, H.-Y. (2011b). *Opt. Expr.* **19,** 18116–18121.
Chen, X., Bhola, B., Huang, Y., and Ho, S. T. (2010). *Opt. Expr.* **18,** 17220.
Chuang, S. L. (2009). Physics of Photonic Devices. second ed. John Wiley & Sons, New Jersey.
De Leon, I., and Berini, P. (2010). *Nat. Photon.* **4,** 382–387.
Dionne, J. A., Sweatlock, L. A., Atwater, H. A., and Polman, A. (2005). *Phys. Rev. B* **72,** 075405.
Dionne, J. A., Sweatlock, L. A., Atwater, H. A., and Polman, A. (2006). *Phys. Rev. B* **73,** 035407.
Ding, Q., Mizrahi, A., Fainman, Y., and Lomakin, V. (2011a). *Opt. Lett.* **36,** 1812–1814.
Ding, K., Liu, Z., Yin, L., Wang, H., Liu, R., Hill, M. T., Marell, M. J. H., van Veldhoven, P. J., Notzel, R., and Ning, C. Z. (2011b). *Appl. Phys. Lett.* **98,** 231108.
Flynn, R. A., Kim, C. S., Vurgaftman, I., Kim, M., Meyer, J. R., Makinen, A. J., Bussmann, K., Cheng, L., Choa, F.-S., and Long, J. P. (2011). *Opt. Expr.* **19,** 8954–8961.
Fujita, M., and Baba, T. (1999). *IEEE J. Sel. Top. Quantum Electron.* **5,** 673–681.
Gargas, D. J., Moore, M. C., Ni, A., Chang, S.-W., Zhang, Z., Chuang, S.-L., and Yang, P. (2010). *ACS Nano* **4,** 3270–3276.
Gather, M. C., Meerholz, K., Danz, N., and Leosson, K. (2010). *Nat. Photon.* **4,** 457–461.
Genov, D. A., Oulton, R. F., Bartal, G., and Zhang, X. (2011). *Phys. Rev. B* **83,** 245312.
Ginzburg, P., Arbel, D., and Orenstein, M. (2006). *Opt. Lett.* **31,** 3288–3290.
Heinzelmann, H., and Pohl, D. W. (1994). *Appl. Phys. A* **59,** 89–101.
Hill, M. T., Oei, Y.-S., Smalbrugge, B., Zhu, Y., de Vries, T., van Veldhoven, P. J., van Otten, F. W. M., Eijkemans, T. J., Turkiewicz, J. P., de Waardt, H., *et al.* (2007). *Nat. Photon.* **1,** 589–594.
Hill, M. T., Marell, M., Leong, E. S. P., Smalbrugge, B., Zhu, Y., Sun, M., van Veldhoven, P. J., Geluk, E. J., Karouta, F., Oei, Y.-S., *et al.* (2009). *Opt. Expr.* **17,** 11110.
Hill, M. T. (2009). Proceedings of SPIE, 7394, Paper, 7394-08 S2, .
Hill, M. T. (2010). *J. Opt. Soc. Am. B* **27,** B36–B44.
Hill, M. T., and Marell, M. J. H. (2011). *Adv. Opt. Technol.* **2011,** 314952.
Hofmann, C. E., Garcia de Abajo, F. J., and Atwater, H. A. (2011). *Nano Lett.* **11,** 372–376.
Huang, J.-S., Callegari, V., Geisler, P., Bruning, C., Kern, J., Prangsma, J. C., Wu, X., Feichtner, T., Ziegler, J., Weinmann, P., *et al.* (2010a). *Nat. Commun.* **1,** 150.
Huang, J., Kim, S.-H., and Scherer, A. (2010b). *Opt. Expr.* **18,** 19581–19591.
Iga, K., Koyama, F., and Kinoshita, S. (1988). *IEEE J. Quantum Electron.* **24,** 1845–1855.
Iga, K. (2000). *IEEE J. Sel. Top. Quantum Electron.* **6,** 1201–1215.
Johnson, P. B., and Christy, R. W. (1972). Optical constants of the noble metals. *Phys. Rev. B* **6,** 4370–4379.
Judkins, J. B., and Ziolkowski, R. W. (1995). *J. Opt. Soc. Am. A* **12,** 1974–1983.
Kim, J., Cha, J.-H., Ha, M.-L., Kim, C.-Y., and Kwon, Y.-S. (2005). Electrochemical Society Proceedings, 361, .
Kim, S.-H., Lee, Y.-H., Huang, J., and Scherer, A. (2009). 11th International Conference on Transparent Optical Networks, ICTON '09, paper Tu.C4.5.
Kim, M. W., and Ku, P.-C. (2011a). *Opt. Expr.* **19,** 3218–3225.
Kim, M. W., and Ku, P.-C. (2011b). *Appl. Phys. Lett.* **98,** 201105.
Knobbe, E. T., Dunn, B., Fuqua, P. D., and Nishida, F. (1980). *Appl. Phys. Lett.* **29,** 2729–2733.
Koenderink, A. F. (2010). *Opt. Lett.* **35,** 4208–4210.
Koller, D. M., Hohenau, A., Ditlbacher, H., Galler, N., Reil, F., Aussenegg, F. R., Leitner, A., List, E. J. W., and Krenn, J. R. (2008). *Nat. Photon.* **2,** 684–687.
Kusunoki, F., Yotsuya, T., Takahara, J., and Kobayashi, T. (2005). *Appl. Phys. Lett.* **86,** 211101.
Kuttge, M., Vesseur, E. J. R., Verhoeven, J., Lezec, H. J., Atwater, H. A., and Polman, A. (2008). *Appl. Phys. Lett.* **93,** 113110.
Kwon, S. H., Kang, J. H., Seassal, C., Kim, S. K., Regreny, P., Lee, Y. H., Lieber, C. M., and Park, H. G. (2010). *Nano Lett.* **10,** 3679–3683.
Lakhani, A. M., Kim, M.-K., Lau, E. K., and Wu, M. C. (2011). *Opt. Expr.* **19,** 18238.

Landau, L. D., and Lifshitz, E. M. (1960). Electrodynamics of Continuous Media. Pergamon Press, Oxford.
Lau, E. K., Lakhani, A., Tucker, R. S., and Wu, M. C. (2009). *Opt. Expr.* **17,** 7790–7799.
Lezec, H. J., Degiron, A., Devaux, E., Linke, R. A., Martin-Moreno, L., Garcia-Vidal, F. J., and Ebbesen, T. W. (2002). *Science* **297,** 820–822.
Li, X. F., and Yu, S. F. (2010). *Opt. Lett.* **35,** 2535–2537.
Liu, H., Wang, B., Leong, E. S. P., Yang, P., Zong, Y., Si, G., Teng, J., and Maier, S. A. (2010). *ACS Nano* **4,** 3139–3146.
Loudon, R. (1970). *J. Phys. A* **3,** 233.
Lu, C.-Y., Chang, S.-W., Yang, S.-H., and Chuang, S. L. (2009). *Appl. Phys. Lett.* **95,** 233507.
Lu, C.-Y., Chang, S.-W., Chuang, S. L., Germann, T. D., and Bimberg, D. (2010). *Appl. Phys. Lett.* **96,** 251101.
Lu, C.-Y., and Chuang, S. L. (2011). *Opt. Expr.* **19,** 13225–13244.
Lu, C.-Y., Chuang, S. L., Mutig, A., and Bimberg, D. (2011a). *Opt. Lett.* **36,** 2447–2449.
Lu, C.-Y., Chang, S.-W., Chuang, S. L., Germann, T. D., Pohl, U. W., and Bimberg, D. (2011b). *IEEE Photon. Technol. Lett.* **23,** 1031–1033.
Ma, R.-M., Oulton, R. F., Sorger, V. J., Bartal, G., and Zhang, X. (2011). *Nat. Mater.* **10,** 110–113.
Maier, S. A. (2006). *Opt. Commun.* **258,** 295–299.
Manolatou, C., and Rana, F. (2008). *IEEE J. Quantum Electron.* **44,** 435–446.
Marell, M. J. H., Smalbrugge, B., Geluk, E. J., van Veldhoven, P. J., Barcones, B., Koopmans, B., Notzel, R., Smit, M. K., and Hill, M. T. (2011). *Opt. Expr.* **19,** 15109–15118.
Maslov, A., and Ning, C. Z. (2007). *Proc. SPIE* **6468,** 646801–646807.
Mayy, M., Zhu, G., Mayy, E., Yakim, A., Webb, A., Livenere, J., Li, H., Bobb, D., and Noginov, M. A. (2009). Conference on Lasers and Electro-Optics (CLEO), paper JTuD199.
Miller, D. (2009). *Proc. IEEE* **97**(7), 1166–1185.
Mizrahi, A., Lomakin, V., Slutsky, B. A., Nezhad, M. P., Feng, L., and Fainman, Y. (2008). *Opt. Lett.* **33,** 1261–1263.
Nagpal, P., Lindquist, N. C., Oh, S. H., and Norris, D. J. (2009). *Science* **325,** 594–597.
Nezhad, M. P., Tetz, K., and Fainman, Y. (2004). *Opt. Expr.* **12,** 4072–4079.
Nezhad, M. P., Simic, A., Bondaenko, O., Slutsky, B., Mizrahi, A., Feng, L., Lomakin, V., and Fainman, Y. (2010). *Nat. Photon.* **4,** 395–399.
Noginov, M. A., Loutts, G. B., Bonner, C. E., Taylor, S., Stefanos, S., Wynne, R. M., and Lasley, B. A. (2000). *J. Opt. Soc. Am. B* **17,** 1329–1334.
Noginov, M. A., Podolskiy, V. A., Zhu, G., Mayy, M., Bahoura, M., Adegoke, J. A., Ritzo, B. A., and Reynolds, K. (2008a). *Opt. Expr.* **16,** 1385–1392.
Noginov, M. A., Zhu, G., Mayy, M., Ritzo, B. A., Noginova, N., and Podolskiy, V. A. (2008b). *Phys. Rev. Lett.* **101,** 226806.
Noginov, M. A., Zhu, G., Belgrave, A. M., Bakker, R., Shalaev, V. M., Narimanov, E. E., Stout, S., Herz, E., Suteewong, T., and Wiesner, U. (2009). *Nature* **460,** 1110–1112.
Nunes, F. D., Vasconcelos, T. C., Bezerra, M., and Weiner, J. (2011). *J. Opt. Soc. Am. B* **28,** 1544–1552.
Omar, M. (1975). Elementary Solid State Physics. Addison-Wesley, Massachusetts.
Oulton, R. F., Sorger, V. J., Pile, D. F. P., Genov, D. A., and Zhang, X. (2008). *Nat. Photon.* **2,** 496–500.
Oulton, R. F., Sorger, V. J., Zentgraf, T., Ma, R.-M., Gladden, C., Dai, L., Bartal, G., and Zhang, X. (2009). *Nature* **461,** 629–632.
Painter, O., Lee, R. K., Scherer, A., Yariv, A., O'Brien, J. D., Dapkusand, P. D., and Kim, I. (1999). *Science* **284,** 1819–1821.
Palik, E. D. (1997). Handbook of Optical Constants of Solids. Academic Press, San Diego.
Perahia, R., Mayer Alegre, T. P., Safavi-Naeini, A. H., and Painter, O. (2009). *Appl. Phys. Lett.* **95,** 201114.
Plotz, G., Simon, H., and Tucciarone, J. (1979). *J. Opt. Soc. Am.* **69,** 419–422.

Prade, B., Vinet, J. Y., and Mysyrowicz, A. (1991). *Phys. Rev. B* **44,** 13556–13572.
Prade, B., and Vinet, J. Y. (1994). *J. Lightw. Technol.* **12,** 6–18.
Protsenko, I. E., Uskov, A. V., Zaimidoroga, O. A., Samoilov, V. N., and O'Reilly, E. P. (2005). *Phys. Rev. A* **71,** 063812.
Ramo, S. J., Whinnery, R., and Van Duzer, T. (1984). Fields and Waves in Communication Electronics. second ed. John Wiley & Sons, New York.
Rosenthal, A. S., and Ghannam, T. (2009). *Phys. Rev. A* **79,** 043824.
Schuller, J. A., Barnard, E. S., Cai, W., Jun, Y. C., White, J. S., and Brongersma, M. L. (2010). *Nat. Mater.* **9,** 193–204.
Seidel, J., Grafstrom, S., and Eng, L. (2005). *Phys. Rev. Lett.* **94,** 177401.
Shantharama, L. G., Schumacher, H., Leblanc, H. P., Esagui, R., Bhat, R., and Koza, M. (1990). *Electron. Lett.* **26,** 1127–1129.
Silver, S. (1949). Microwave Antenna Theory and Design. McGraw-Hill, New York.
Sirtori, C., Gmachl, C., Capasso, F., Faist, J., Sivco, D. L., Hutchinson, A. L., and Cho, A. Y. (1998). *Opt. Lett.* **23,** 1366–1368.
Stockman, M. I. (2010). *J. Opt.* **12,** 024004.
Stockman, M. I. (2011). *Opt. Expr.* **19,** 22029–22106.
Taflove, A., and Hagnes, S. C. (2005). Computational Electrodynamics: The Finite Difference Time Domain Method. third ed. Artech House, Boston.
Tanaka, K., and Tanaka, M. (2003). *Appl. Phys. Lett.* **82,** 1158–1160.
Tanaka, K., Tanaka, M., and Sugiyama, T. (2005). *Opt. Expr.* **13,** 256–266.
Theye, M. L. (1970). *Phys. Rev. B* **2,** 3060–3078.
Urbanczyk, A., Hamhuis, G. J., and Notzel, R. (2010). *Appl. Phys. Lett.* **97,** 043105.
Visser, T. D., Blok, H., Demeulenare, B., and Lenstra, D. (1997). *IEEE J. Quantum. Electron.* **33,** 1763–1766.
Walther, C., Scalari, G., Amanti, M. I., Beck, M., and Faist, J. (2010). *Science* **327,** 1495–1497.
Wang, F., and Ron Shen, Y. (2006). *Phys. Rev. Lett.* **97,** 206806.
Walters, R. J., Van Loon, R. V. A., Brunets, I., Schmitz, J., and Polman, A. (2009). *Nat. Mater.* **9,** 21–25.
Wang, Y.-G., Chen, C.-C., Chiu, C.-H., Kuo, M.-Y., and Shih, M. H. (2011a). *Appl. Phys. Lett.* **98,** 131110.
Wang, H., Sun, M., Ding, K., Hill, M. T., and Ning, C.-Z. (2011b). *Nano Lett.* **11,** 1646–1650.
Yarborough, J. M. (1974). *Appl. Phys. Lett.* **24,** 629–630.
Yu, K., Lakhani, A., and Wu, M. C. (2010). *Opt. Expr.* **18,** 8790.
Zia, R., Selker, M. D., Catrysse, P. B., and Brongersma, M. L. (2004). *J. Opt. Soc. Am. A* **21,** 2442–2446.